Realistic Single-Shot and Long-Term Collision Risk for a Human-Style Safer Driving

Lingguang Wang[1], Carlos Fernandez Lopez[1] and Christoph Stiller[1]

***Abstract*— Navigation in congested environments is a challenge for autonomous vehicles and they should consider collision risk metric into their driving behavior. In this paper, we propose a novel two-fold indicator: On the one hand, single-shot risk works in space domain, considering geometries, locations and the velocities of the obstacles in the current scene. On the other hand, long-term risk considers the evolution of the current scene and provides risk values in time domain. The map information and different prediction models (e.g. reachable sets, probabilistic) are considered in the long-term risk, which can then be used in trajectory planning or decision making approaches. Our method can be applied to scenarios with arbitrary road topologies (intersections, roundabouts, highway, etc.) and it is suitable regardless of the scene prediction method. We formulate the single-shot (or short-term) risk with one single function fitted using Monte Carlo (MC) Simulations. The results are evaluated in real scenarios using HighD dataset and compared with other risk indicators such as THW and TTC. In addition, it is applied to a simple trajectory planner in order to demonstrate that the proposed approach imitates human driving style.**

I. INTRODUCTION

Every year millions of people worldwide have traffic accidents with a high number of fatalities. Safer cars on crashes and progressively integration of ADAS into medium-cost vehicles has been reducing the severity of the accidents. However, current ADAS and autonomous driving are not safe enough. Since autonomous vehicles have been deployed in open traffic, some accidents were caused because of misdetections or errors on other road-participants intention prediction.

Despite safety is the most important topic concerning autonomous driving, there are other terms such as driving comfort and utility of transportation to consider. When safety is the most important term, the vehicle could lead in a too conservative behaviour with frequent stops and therefore making the trip less useful and comfortable. Therefore, a correct balance between these three terms should be properly adjusted to make autonomous vehicles safer, more comfortable and useful.

In order to maintain sufficient safety, the collision risk of the vehicle should be minimized and limited, which is understood as a two-fold term in this paper. The first term embraces single-shot risk, where all the map information and possible intentions of other traffic participants are neglected and collision risk is only derived from the current scene, assuming that the shapes, locations and motions of all the obstacles are given despite noisy sensor data. The single-shot risk represents the probability that the 2 observing vehicles will collide if their short-term future motion deviate from the expected motion. Since it's difficult to compute this collision probability analytically, we use MC simulations [1] to simulate the collision rate and then fit function to it. Assuming that the ego vehicle and obstacle change their driving direction and velocity randomly in the short-term future, as dipicted in Fig. 1, we record the collision rate after a large amount of simulation trials as ground truth value for the function.

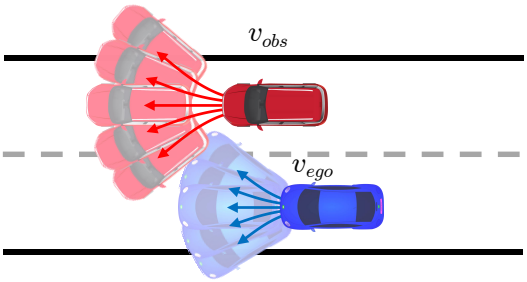

Fig. 1: Possible short-term future movement of ego vehicle (blue) and obstacle (red).

The second term contains the long-term risk. The length of this long-term risk depends on what is the prediction horizon of the scene prediction model. Due to the uncertainty, complexity and unpredictability of other traffic participants, this paper is focused on the single-shot risk measurement. Specific pedestrian, cyclist or car prediction methods can be considered in this term as well as the general-scene prediction ones. Regardless the prediction method, the same single-shot risk assessment can be applied for each scene at different time steps. The collision risk for the whole prediction horizon is the weighted maximum of all single-shot risks under the assumption that the further the time step is, the smaller the single-shot risk is weighted. The reason for this assumption will be explained in Section III.

II. RELATED WORK

Collision risk has been the focus of research since decades. The most common approach to measure collision risk is using Time-To-Collision (TTC) [2]. It is mainly suitable for car following on straight roads and it is computed assuming all the obstacles remaining constant velocities and all the map information, traffic rules and interactions are ignored. Furthermore, it only measures relative speed and as

[1]Lingguang Wang, Carlos Fernandez Lopez and Christoph Stiller are with the Institute of Measurement and Control Systems, Karlsruhe Institute of Technology (KIT), Karlsruhe, Germany lingguang.wang, carlos.fernandez, stiller@kit.edu

a consequence, two vehicles driving at constant high speed with constant close distance between them have a small TTC, which does not reflect the real risk of driving close to each other at high speeds.

Some authors compute collision risk deterministically [3], [4] using distance between two traffic participants as a metric. However, Uncertainty of the future motion of the vehicles plays an important role, thus the collision risk can also be computed in a probabilistic manner [5]. Some simplify the reachable sets of the vehicle to geometric shapes and calculate the percentage of the overlap between the shapes as risk indicator [6]. Some approaches propose to model the future motion of the vehicle as normal distribution and compute the collision probability relying on the minimum of the distance function and statistical linearization via the unscented transformation [7], while some recent works present analytic solutions for calculating collision probability [8]. These approaches treat motion prediction and risk assessment independently, thus including interactions and road geometries becomes possible. However, they either neglect the geometry of the vehicle or simplify it to ellipse to reduce the computational complexity. A more serious problem is that these approaches ignore the impact of the velocities of ego vehicle and obstacles on the collision risk. For instance, the collision probability should be higher if we pass by a static object with higher velocity, because a slight deviation in the driving direction is more likely to cause a collision as we have less reaction time for correction.

Some recent works [9], [10] use risk level sets to represent the congestion cost that maps the density and motion of vehicles to an occupancy risk. However this approach is only evaluated on a straight highway scenario and it does not cooperate with predictions, which results in preferring behavior that has lower current risk but not future risk.

A more general approach [11] derives the expression for computing the collision probability rate and obtains the collision probability by numerical integration over time, which analytically solves the problem but does not consider extended obstacles.

This paper aims to provide collision risk that: 1) is easy to compute, 2) doesn't exactly matches the ground truth but is practical and realistic in the sense of generating human-like behavior, 3) considers not only the positions and simplified geometries (e.g.points, circles) of the ego vehicle and the obstacles but also more dimensions, e.g. rectangle shape, velocity and prediction.

In comparison with the previous works, we could state the novel contributions of our approach:

- It works with arbitrary prediction models, e.g. set-based [12], probabilistic with any type of distribution, lane-based [13], etc.. Therefore, arbitrary road topologies and traffic rules are possible to include.
- It formulates single-shot collision risk as simple derivable function of location, orientation and velocity by fitting the function to the ground truth collision probabilities that are produced by MC simulation.
- It takes not only relative pose but also relative velocity into account, which achieves human-like driving behaviors, e.g. slowing down when passing static obstacles, slowing down and move to the side when encountering high speed oncoming vehicle, etc..

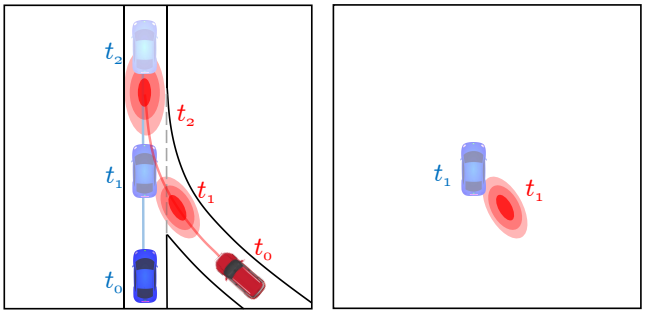

(a) Evolution of the scene. (b) Single-shot scene

Fig. 2: Scene evolution. Blue vehicle corresponds with the ego-vehicle and the red one belongs to other road participants. Red ellipses are probabilistic predictions of scene evolution.

The remainder of this paper is organized as follows: Section III formulates the problem and introduce the overall approach. Section IV details how the single-shot risk function is formulated and the parameters are learned from MC simulation. Section V presents some evaluations on the highD datasets [14] and proof-of-concept planning in several real-life scenarios. Finally, conclusions and future work are discussed in Section VI.

III. PROBLEM FORMULATION

Given the single-shot scene $\mathcal{S}$, see Fig. 2b, which contains the ego vehicle, detected and tracked obstacles and their distributions, our method should provide one single value that indicates how probably a collision will happen in the near future. We define this as single-shot risk R_s. Given the current decision (or trajectory) of the ego vehicle and the High-Definition (HD) Map, e.g. Lanelet2 [15], by assuming that other vehicles follow certain driving pattern (reachable set, probabilistic, lane-based, etc.) and the ego vehicle follows its own plan, the traffic scene could be predicted in relative long-term as depicted in Fig. 2a. We define the probability of having a collision during the whole prediction horizon as long-term risk R_l.

Obviously, the evolution of the scene $\mathcal{S}$ can be formulated as a function S of the map information $\mathcal{M}$, the prediction pattern $\mathcal{P}$ and the time t. In order to preserve the possibility of using interactive prediction model, the prediction pattern $\mathcal{P}$ should also be a function of the action or the plan of the ego vehicle $\mathcal{A}$. Thus the scene at time t can be written as

$$\mathcal{S}_t = S(\mathcal{M}, \mathcal{P}(\mathcal{A}), t) \tag{1}$$

Therefore, the long-term risk R_l can be formulated as:

$$\begin{aligned} R_l &= \max_{k=0,\dots,K} \gamma^k R_s(S(\mathcal{M}, \mathcal{P}(\mathcal{A}), t_k)) \\ &= \max_{k=0,\dots,K} \gamma^k R_s(\mathcal{S}_{t_k}) \end{aligned} \tag{2}$$

where k is the time step and K is the total number of prediction steps. γ denotes the discount factor of the future single-shot risk. This is a hyperparameter which affects how much weight given to future single-shot risk in the long-term risk, similar to the idea of the discount factor in the reward function of reinforcement learning [16]. γ should be set between $[0, 1]$. However, in the context of long-term risk assessment, γ has a practical meaning. Even if we expect high future risk, given that we have more reaction time to avoid the critical situation, the real risk should be lower, i.e. the discount factor should depend on the evasive options the ego vehicle has, which matches the definition of Time-To-React (TTR). As this is not the focus of this paper, we take the simplification of (2) and preserve the possibility for further improvement (e.g. integrating TTR into the long-term risk) in the future work.

IV. SINGLE-SHOT RISK

Given the state of the ego vehicle and the distributions of the obstacles, the single-shot risk represents the collision probability with any of the obstacles in the short future. Before formulating the risk function, two assumptions are made for computational simplification. It is first assumed that the trajectory of the ego vehicle is deterministic, as the localization and control error is usually negligible compare to the detection and prediction of other obstacles. With this assumption we can express the single-shot risk of the ego vehicle with the distribution of j-th obstacle at time t_k as:

$$R_s(O^j_{t_k}) = \int_x \int_y \int_\varphi \int_v P(C|x, y, \varphi, v) D^j_{t_k}(x, y, \varphi, v) \, dx dy d\varphi dv \tag{3}$$

where $D^j_{t_k}$ represents the probability density function (PDF) of j-th obstacle at time t_k. $P(C|x, y, \varphi, v)$ is the collision probability with the obstacle in the short future, which has the position (x, y), orientation φ and velocity v. This probability is the key function in the single-shot risk and will be discussed in detail in Section IV-A. Note that there are still 4 dimensions in the integral, which makes the analytically not solvable integral even more complicated. Therefore we introduce another assumption. As the obstacles always follows the lane and thus the variance of the orientation is small, the orientation can be assumed as deterministic. However, the variance of the velocity inside one distribution can be large if the uncertainty of the acceleration is high, the same assumption cannot be made. But for certain types of prediction (e.g. set-based), some reasonable simplifications can still be adopted.

In order to compute (3), the distribution of j-th obstacle at time t_k is discretized. Fig. 3 illustrates the discretized reachable sets predicition and probabilistic prediction of the obstacle. The former is a special case of the latter. Reachable set can be regarded as a set of occupancy grids, within which the existence probability of the obstacle is 1. We divide the x coordinate along the centerline of the lane into $N-1$ slices and each slice represents one virtual obstacle at the position

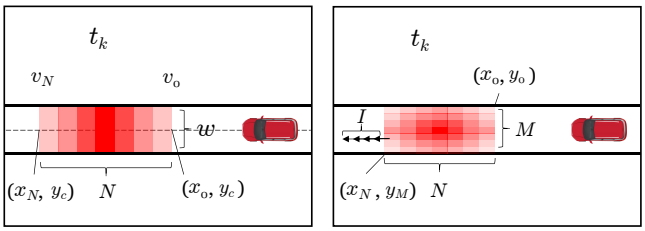

(a) Reachable set prediction. (b) Probabilistic prediction.

Fig. 3: Discretization of the predictions.

(x_n, y_c), with orientation parallel to the centerline φ_c, width w, the original obstacle length and the existence probability 1. The velocity v of n-th virtual obstacle can be linearly interpolated and expressed as $v_n = v_0 + \frac{n}{N}(v_N - v_0)$, where v_0 and v_N are the velocities after time t_k with full brake and full acceleration. We take the maximum risk among all the virtual obstacles as the single-shot risk with this reachable set. Thus for Fig. 3(a), (3) can be rewritten as:

$$R_s(O^j_{t_k}) = \max_{n=0,\dots,N-1} P(C|x_n, y_c, \varphi_c, v_n) \tag{4}$$

For probabilistic prediction, the distribution in space is divided into $(M-1) * (N-1)$ grids and the velocity in each grid is discretized into $I-1$ values. Thus, (3) can be rewritten as:

$$R_s(O^j_{t_k}) = \sum_{i=0}^{I-1} \sum_{m=0}^{M-1} \sum_{n=0}^{N-1} P(C|x_n, y_m, \varphi_c, v_i) P(x_n, y_m, v_i) \tag{5}$$

where $P(x_n, y_m, v_i)$ can be analytically solved with (6).

$$P(x_n, y_m, v_i) = \int_{x_n}^{x_{n+1}} \int_{y_m}^{y_{m+1}} \int_{v_i}^{v_{i+1}} D^j_{t_k}(x, y, v) dx dy dv \tag{6}$$

and (7) should hold

$$\int_{x_0}^{x_N} \int_{y_0}^{y_M} \int_{v_0}^{v_I} D^j_{t_k}(x, y, v) \, dx dy dv = 1 \tag{7}$$

The goal is to obtain the collision probability with all the obstacles in the scene $\mathcal{S}_{t_k}$ at time t_k. As the interaction between ego vehicle and the obstacles are difficult to model, we assume that the collision events with all the obstacles are independent. Therefore the probability of collision with any of the obstacle at time t_k, i.e., the probability of collision happens between ego vehicle and any of the obstacles in the scene at time t_k, can be computed following (8).

$$R_s(\mathcal{S}_{t_k}) = 1 - \prod_{j=0}^{J} (1 - R_s(O^j_{t_k})) \tag{8}$$

A. Fitting Collision Probability Function to MC Simulation

The only problem left is $P(C|x, y, \varphi, v)$ in (4) and (5), i.e. collision probability with one obstacle in short term, which has the state (x, y, φ, v) with known width and length.

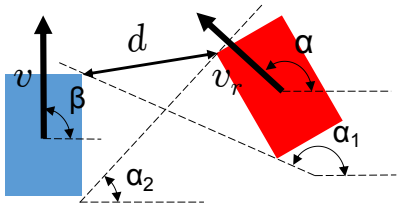

Fig. 4: Chosen features as the input of the risk function for single configuration of ego vehicle (blue) and obstacle (red).

As mentioned in Section I, this probability represents the chance that the 2 vehicles will collide if their short-term future motion (driving direction and velocity) deviates from the expected motion. We use rectangles to represent the shape of the vehicles. Note that the collision probability will be 1 if the shapes of two vehicles already intersects before applying short-term prediction. With "short-term" or "in the short future" we choose 0.2 seconds in this paper, which reflects roughly the optimal reaction time of an experienced autonomous driving system [17]. As assumed in Section III, the state of the ego vehicle at each time step is known given the own plan. $P(C|x, y, \varphi, v)$ is basically the same as $P(C|Configuration)$. Under configuration we mean a combination of two vehicles that possess specific position, orientation, size and velocity. In order to achieve real-time capability, this probability should be express as a simple function, which we call risk function in the rest of the paper. Ideally, a large number of MC simulation (10000 is chosen according to [1]) can provide enough information. We randomize the vehicles' yaw rate $\dot{\varphi}$ and longitudinal acceleration a in the next 0.2 seconds as normal distribution which follow $\dot{\varphi} \sim \mathcal{N}(0, 0.3)$ and $a \sim \mathcal{N}(0, 4.0)$. The collision rates from the MC simulations are considered as ground truth and we try to fit appropriate risk function to that.

To do so, we propose an initial risk function heuristically. After that, a large amount of ground truth collision rates from random configurations will be generated. Then the remaining unknown parameters in the function will be fine-tuned or so called "learned" via gradient descent with the help of the Tensorflow Framework [18], using the deviation of the output values as loss.

The features that are chosen as the input of the risk function are shown in Fig. 4. v and v_r are velocity of the ego vehicle and relative velocity respectively. d is the distance between 2 rectangles. α and β denote the relative velocity angle and the driving direction of the ego vehicle. α_1 and α_2 are the angles of two inner tangent lines of two rectangles. Once α is between α_1 and α_2, it is more likely that the two rectangles will collide in the near future following the current motion. Thus they are also called critical relative angles later.

Intuitively, the collision probability should be high if two vehicles have high v_r and are close (i.e. with small d), and simultaneously are driving towards each other (i.e. α close to the middle of two critical relative angles α_1 and α_2). With this idea, the first part of the risk function P_1 can be proposed as $f(v_r, d)g(\alpha, \alpha_1, \alpha_2)$. f reflects how close and how fast two vehicles drive with respect to each other. g shows how straight two vehicle drive towards each other. However, if 2 vehicles drive parallel to each other with high absolute speed and 0 relative speed, the risk should also be high if they are close enough, as a small deviation of the driving direction to the wrong side will cause collision in the near future. But in P_1, f and g will be small as v_r is 0 and they are not driving towards each other. Therefore, P_1 alone is not enough and the second part $P_2 = (1 - f(v_r, d))h(v, d)z(\beta, \alpha_1, \alpha_2)$ is necessary. $(1 - f(v_r, d))$ gets bigger when f is small. h should be high if they drive fast (i.e. high v) and close (i.e. small d). z models how the collision probability changes with the relative position of the obstacle to the ego vehicle.

Given the aforementioned heuristics, the risk function is defined as (9).

$$\begin{aligned} &P(C|Configuration) \\ &\quad = P_1 + P_2 \\ &\quad = f(v_r, d)g(\alpha, \alpha_1, \alpha_2) + \\ &\qquad (1 - f(v_r, d))h(v, d)z(\beta, \alpha_1, \alpha_2) \end{aligned} \tag{9}$$

In order to obtain the exact expression of all the unknown functions in (9), some typical configuration patterns of two vehicles will be studied. In Fig. 5, changing one feature and fixing the other ones, it can be observed how the pattern of short-term collision probability varies using MC simulations. After choosing appropriate functions and calculating the collision rates for the same configurations, the fitted values are plotted in the same figures which shows only minor variations to the ground truth. Note that the curves in Fig. 5(b) and Fig. 5(d) from MC simulation is discontinuous and highly irregular due to the fact that the α_1 and α_2 have sudden jumps when α_r changes.

The final functions can be expressed as:

$$f(v_r, d) = sigmoid(\frac{\lambda_1(\lambda_2 v_r - d)}{v_r}) \tag{10}$$

$$\begin{aligned} g(\alpha, \alpha_1, \alpha_2) = sigmoid(\lambda_3(\alpha_2 - \alpha)) - \\ sigmoid(\lambda_3(\alpha_1 - \alpha)) \end{aligned} \tag{11}$$

$$h(v, d) = 2 * sigmoid(-\frac{\lambda_4 d}{v}) \tag{12}$$

$$z(\beta, \alpha_1, \alpha_2) = e^{-\lambda_5(|\frac{\alpha_2 - \alpha_1}{2} - \beta| - \lambda_6)^2} \tag{13}$$

The unknown parameters λ_1 to λ_6 are estimated to fit the simulated results. We use sigmoid functions because they are fast to compute derivatives of the features and it is an important requirement to make the system real-time capable.

B. Parameter Learning

Since the features influence on the collision rate is only observed independently, and they cannot be guaranteed as uncorrelated to each other, the λ_1 to λ_6 should be fine-tuned with all the above functions combined as a whole risk function to ensure a low error to the MC simulation.

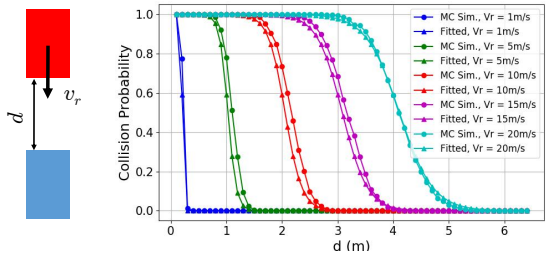

(a) Fitting function f by changing d and v_r

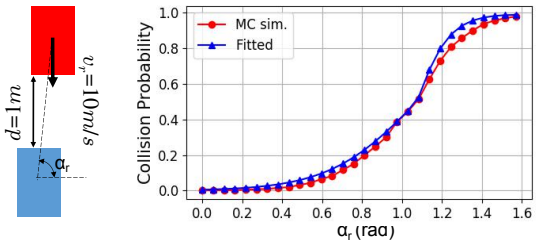

(b) Fitting function g by changing α_r with fixed d and v_r

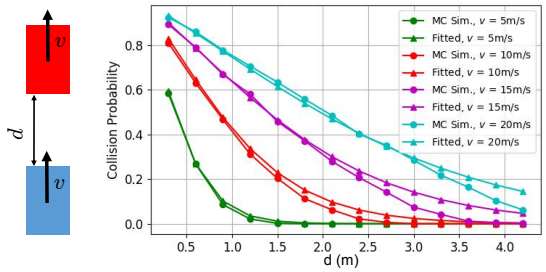

(c) Fitting function h by changing d and v

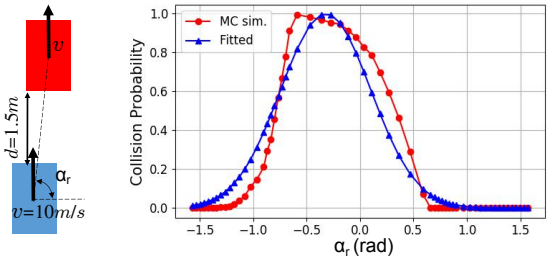

(d) Fitting function z by changing α_r with fixed d and v

Fig. 5: Fitting functions in (9) to the results of MC simulations. The curves with dots are the collision rates from the MC simulations. The curves with triangles show the collision rates from the fitted functions with the same vehicle configuration.

We generate another 10000 ground truth collision rates from the MC simulation, yet with totally random configurations (d, v_r, etc.) instead of manually designed ones. The Tensorflow Framework is utilized as optimization tool for tuning the optimal weights λ_1 to λ_6. The Mean Square Error (MSE) between the fitted collision rates from (9) and the ground truth is used as loss. After 10000 training steps with 0.01 learning rate and the standard gradient descent algorithm, the final mean error of the collision rate over all the 10000 data is 0.07. Table I presents the final values of λ_1 to λ_6.

TABLE I: Optimal values of the weights

Parameter	λ_1	λ_2	λ_3	λ_4	λ_5	λ_6
Value	21.0	0.186	-8.47	50.0	1.6	1.5

V. EVALUATION

For showing the effectiveness of our approach on real data and also on generating human-like driving behavior, evaluations on both real data and on simulated proof-of-concept planner were done.

A. Evaluation on HighD Dataset

HighD dataset provides highly accurate trajectories of a large amount of vehicles at different highway segments in Germany. There are data from different scenarios recorded, e.g. follow driving, mandatory merging, sudden braking, lane changes, etc., which are suitable for risk assessment on structured roads.

1) Statistic Analysis: For follow driving, we compare our long-term risk R_l to the commonly used TTC and Time Headway (THW), which are directly provided by the datasets.

We examined 7826 vehicles from Track 20 to Track 27 in the dataset, which include all possible scenarios (traffic jams, merging and free driving). The long-term risk R_l is computed with (2) for all the vehicles at each frame, and the maximum R_l over all the frames along the track is chosen for each vehicle. As comparison, the minimum TTC and THW along the track are also read from the dataset. Fig. 6 illustrates the distributions of the TTC and THW for vehicles of different risk levels according to our risk assessment.

For computing R_l, we use time-to-stop (with deceleration $-7m/s^2$) as prediction time, which is dynamic depending on the velocity of the vehicle.

The time interval between each prediction step is 0.2 seconds, which matches the short-term prediction time of the single-shot risk. The discount factor γ in (2) is manually set to 0.9 but its optimality still needs to be adjusted according to the scene, as mentioned in Section III.

For other vehicles, the reachable sets prediction along the current lane with $a_{min} = -7m/s^2$ and $a_{max} = 5m/s^2$ is utilized. For ego vehicle, the longitudinal action consists of two parts, i.e. following current acceleration for 0.2 seconds and applying full brake ($-7m/s^2$) for the rest of the prediction time, assuming that it follows the recorded path which is already known from the data. If this longitudinal action cannot prevent interfering with the reachable sets of the front vehicle, the long-term risk R_l should be considered as high, which means if the front vehicle takes emergency braking for unknown reasons, the ego vehicle can hardly avoid a collision with it. According to the Responsibility-

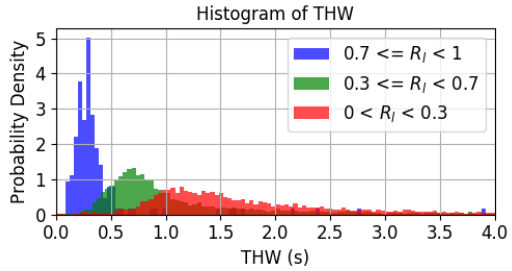

(a) Histogramms of the THW for vehicles of different risk levels

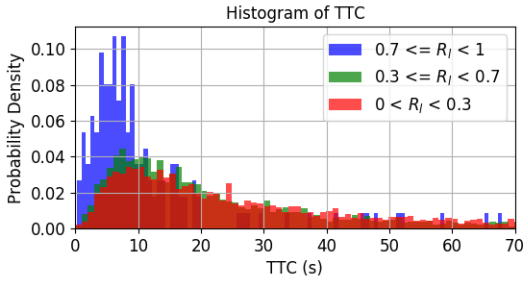

(b) Histogramms of the TTC for vehicles of different risk levels

Fig. 6: Histogramms of the THW and TTC for vehicles of different risk levels.

Sensitive Safety (RSS) [19] from Mobileye, we neglect the vehicles behind, which are responsible for the collision if they hit the ego vehicle from the back.

On the one side, long-term risk R_l distribution fits to THW distribution, i.e. highly risky vehicles according to our risk measurement usually have lower THW (see Fig. 6(a)). On the other side, according to Fig . 6(b) the R_l is not strongly correlated with TTC. TTC is not a good metric because one vehicle following another one at 1 meter distance at the same high-speed has TTC=0 and still is a risky situation. Despite THW and our long-term risk R_l are correlated in the HighD data, THW cannot be applied to scenarios where lane changes are involved or vehicles are not driving on the same lane, or where there is even no clear division of the lane.

2) Case Study: For the evaluation of lane changes and merging, the one dimensional TTC and THW is not enough. Therefore we study some highly risky cases in addition to the trends and distribution analysis. We focus on the Track 25 in the dataset, which records a starting point of a traffic jam on the highway. In this scenario, the vehicle needs to decelerate aggressively, make evasive lane changes and passing with high relative speed frequently. Table II lists some examples in Track 25 where the long-term risk R_l is extremely high with some details of the most risky frame. Note that we only consider examples that are not in vehicle following scenario. The high risks are usually caused by passing obstacle extremely close with high velocity difference.

As Fig. 7(a) shows, the vehicle with id 1318 follows a truck with a very small distance during high speed driving, which is considered as critical because a slight change in the driving direction of the truck or a small control error of the ego vehicle might cause collision. Fig. 7(b) and Fig. 7(c) depict an passive evasive lane change and an offensive overtaking at high speed, which are also considered as highly risky from the perspective of a human driver.

These examples show that using our approach, we can identify risky situations that are reasonable and understandable to humans.

TABLE II: Examples of highly risky vehicles

Max. R_l	Id of ego vehicle	minimum neighbor distance (m)	ego v (kph)	obstacle v (kph)	Description
0.86	1318	0.46	97.2	94.6	passing truck close and fast
0.90	1380	0.7	27.0	18.0	evasive lane change with small distance
0.92	1491	0.53	106.2	86.7	overtaking truck close and fast

B. Evaluation with Proof-of-Concept Planner

In order to prove that by minimizing the long-term risk R_l, a human-like driving behavior is achieved, we do proof-of-concept planning in different scenarios.

We do path-velocity decomposition for our planner. We first generate cubic splines π in Frenét Frame [20] with different lateral offsets from the center line. On the candidate paths, different accelerations a are sampled (between $-7m/s^2$ and $5m/s^2$ with $0.05m/^2$ step size), and the ego vehicle follows the same acceleration for the whole planning horizon 5s. For each combination of acceleration and path (a, π), one corresponding cost is associated, which balances comfort, utility and safety. For guaranteeing safety, the other obstacles are predicted using reachable sets.

The cost for (a, π) is formulated as:

$$\begin{aligned} Cost(a,\pi) =& w_1 a^2 + w_2(a-a_l)^2 + w_3(d(\pi)-d(\pi_l))^2 + \\ & w_4(1-k\frac{a}{a_{max}}-\frac{v}{v_d})^2 + \\ & w_5 R_l(a,\pi)^2 + w_6 d(\pi)^2 \end{aligned} \tag{14}$$

where w_1 to w_6 denote the weights for balancing comfort (w_1 for acceleration, w_2 for jerk, w_3 for variation of path), utility (w_4 for maintaining desired velocity) and safety (w_5 for collision risk, w_6 staying in the center of the lane). a_l and π_l are the chosen acceleration and spline at the last planning step. To maintain the desired velocity v_d, we adapt the idea of a proportional control (P-Controller), i.e. the ratio of the expected acceleration to the maximum acceleration a_{max} should be proportional to the deviation of the current velocity from v_d, and wrong acceleration is penalized correspondingly. $d(\pi)$ is the lateral offset of the path π to the center line.

After tuning the weights, the action (a, π) with the lowest cost is selected for each planning step, and the replanning is

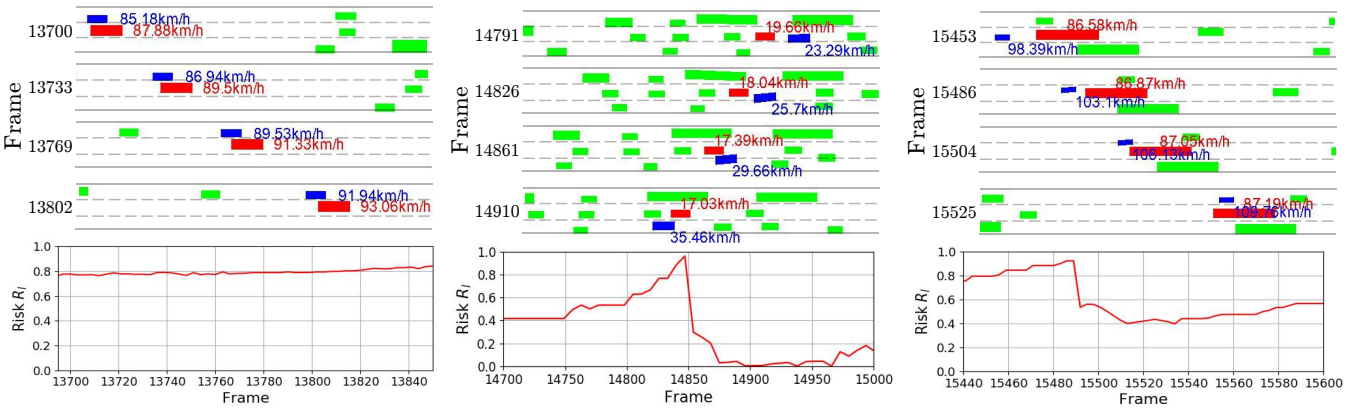

(a) Vehicle id 1318. (b) Vehicle id 1380. (c) Vehicle id 1491.

Fig. 7: Highly risky vehicles and their critical frames. Blue vehicle is the ego vehicle with its velocity also shown in blue. Red vehicle is the most critical obstacle in the scenario with its velocity shown in red. Green vehicles are other obstacles.

done with 20Hz. The planner is tested in several scenarios and the simulation results are shown in Fig. 8.

1) Driving on multi-lane road: In Fig. 8(a), the first scenario simulates how the vehicle avoids risky situation with human-style on a road with 2 lanes leading to the same direction and one oncoming lane, as depicted in Fig. 8a. As the ego vehicle is close to the green vehicle (with $9m/s$) initially, it tries to move to the left a little to enlarge the distance at t_0. After the oncoming red vehicle (with $9m/s$) comes closer, the ego vehicle intends to stick to the right bound of the lane and reduce the velocity at t_1, as the risk caused by the red vehicle is way larger than by the green one because of the larger relative velocity. Finally, the ego vehicle returns to the middle of the lane after passing the red vehicle at t_2. With the approach in [9], the ego vehicle is not able to ajust its lateral position or longitudinal velocity, since the risk caused by both obstacles will be equal and reducing the ego velocity doesn't help reduce the collision risk.

2) Overtaking cyclist: In Fig. 8(b), while approaching the cyclist ($6m/s$) from the back with $9m/s$, the ego vehicle reduces the speed a little to avoid passing the cyclist with high relative speed, which could lead to high collision risk. Meanwhile, the ego vehicle also tries to stick to the left bound and pass with as large distance as possible.

3) Passing static obstacle: In Fig. 8(c), the black obstacle simulates a row of parked vehicles which narrows the road a little. In order to not crush into them due to unexpected oscillation of the steering wheel or control errors, the ego vehicle reduces the speed and moves to the left side of the road. After passing them, it recovers its speed and lateral position on the lane. In the approaches of [8] and [9], the static obstacles are not able to cause considerable risk since the location and orientation are more deterministic. Thus, the same human-style behavior is difficult to obtain without other manually designed costs.

4) Passing static obstacle with oncoming vehicle: The scenario described in Fig. 8(d) often occurs on narrow rural roads that are difficult to pass two vehicles side by side when there are parked vehicles. As a human driver is not sure whether the corridor is enough for two vehicles, they always reduce the speed and stick to the right side to make room for the oncoming vehicle (red) and let it pass first. The maximum risk occurs at the time where they meet each other. With our approach, this human-like behavior is perfectly replicated in simulation. We can also adjust the weights in the cost function to simulate different level of conservative or offensive drivers.

To sum up, with most of the two-dimensional risk assessment approaches, e.g. [8], [9], [13], the ego vehicle is still able to round the obstacles with larger distance, adjusting the velocity simultaneously is however not possible, because their risk measurements don't take the relative velocity of the ego vehicle and the obstacles into account.

VI. CONCLUSION AND FUTURE WORK

This paper is motivated with the purpose of providing realistic single-shot (or short-term) risk and long-term risk for not only fully automated vehicles as in our simulation evaluations, but also for level 1-4 ADAS, e.g. risk monitoring system, collision warning system. Our approach can even potentially be applied for other traffic participants that follow certain motion model, e.g. motorcycle, bicycle, by only adopting the MC simulation and fitting other risk functions to them.

Our approach can be applied to scenarios with arbitrary road topologies (intersections, roundabouts, highway, etc.) and it is suitable regardless the prediction method. It is not only more robust than traditional one-dimensional risk indicators, e.g. THW and TTC, but also more realistic than most of the two-dimensional collision risks.

In this paper, the weights in (14) are fitted to imitate human-like behavior. However, we plan to learn the weights from real datasets in order to obtain real human-like behaviors. By dividing the data into different driving styles (conservative, offensive), different combinations of weights can be learned to replicate those driving styles in simulation or even in real driving test.

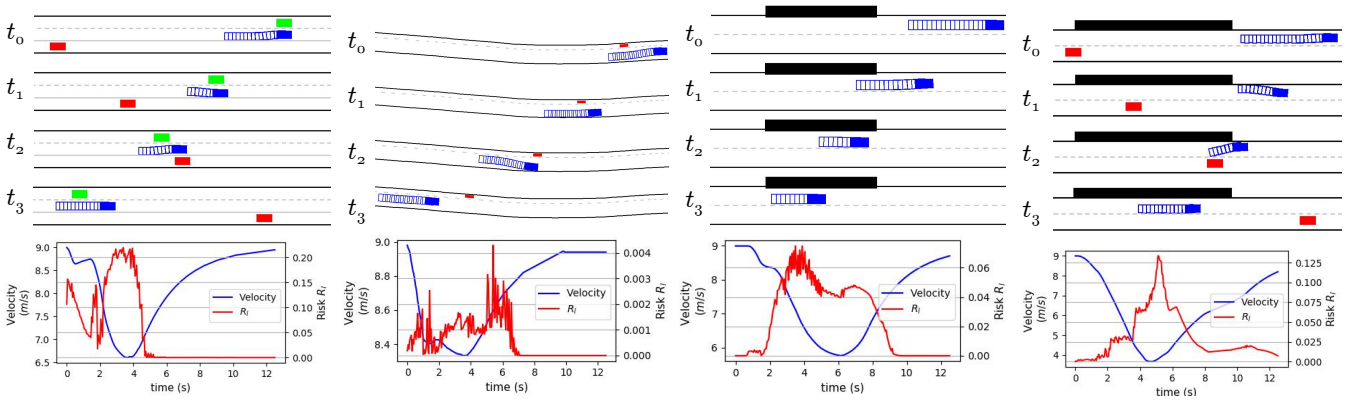

(a) $t_0 = 0s$, $t_1 = 2.25s$, $t_2 = 4.25s$, $t_3 = 6.8s$ (b) $t_0 = 0s$, $t_1 = 2.25s$, $t_2 = 4.25s$, $t_3 = 6.8s$ (c) $t_0 = 0s$, $t_1 = 2.25s$, $t_2 = 4.4s$, $t_3 = 6.6s$ (d) $t_0 = 0s$, $t_1 = 2.25s$, $t_2 = 4.5s$, $t_3 = 7.0s$

Fig. 8: Planning for ego vehicle (blue) in different scenarios with initial velocity $9m/s$. (a) Driving parallel to a vehicle (green) with one oncoming vehicle (red). (b) Overtaking one cyclist (red). (c) Passing static obstacle (black). (d) Passing static obstacle (black) with one oncoming vehicle (red).

Another potential improvement is the strategy used for computing the long-term risk in (2). As mentioned in Section III, we can introduce TTR that considers the time within which safe actions are still available.

Finally, we want to integrate this method in our prototype vehicle for collision risk monitoring in real world scenarios. Furthermore, we will integrate our approach in our current two-dimensional optimization based trajectory planner to obtain less risky trajectories.

ACKNOWLEDGMENT

This work is accomplished within the project "UNICARagil" (FKZ 16EMO0287) and the financial support from the Federal Ministry of Education and Research of Germany (BMBF) is acknowledged.

REFERENCES

[1] A. Lambert, D. Gruyer, and G. Saint Pierre, "A fast monte carlo algorithm for collision probability estimation," in *2008 10th International Conference on Control, Automation, Robotics and Vision*, Dec 2008, pp. 406–411.

[2] D. Lee, "A theory of visual control of braking based on information about time-to-collision," *Perception*, vol. 5, pp. 437–59, 02 1976.

[3] F. Damerow and J. Eggert, "Balancing risk against utility: Behavior planning using predictive risk maps," in *2015 IEEE Intelligent Vehicles Symposium (IV)*, June 2015, pp. 857–864.

[4] P. Raksincharoensak, T. Hasegawa, and M. Nagai, "Motion planning and control of autonomous driving intelligence system based on risk potential optimization framework," *International Journal of Automotive Engineering*, vol. 7, pp. 53–60, 03 2016.

[5] S. Lefevre, D. Vasquez, and C. Laugier, "A survey on motion prediction and risk assessment for intelligent vehicles," *Robomech Journal*, vol. 1, 07 2014. [Online]. Available: https://doi.org/10.1186/s40648-014-0001-z

[6] D. Greene, J. Liu, J. Reich, Y. Hirokawa, A. Shinagawa, H. Ito, and T. Mikami, "An efficient computational architecture for a collision early-warning system for vehicles, pedestrians, and bicyclists," *IEEE Transactions on Intelligent Transportation Systems*, vol. 12, no. 4, pp. 942–953, Dec 2011.

[7] A. Berthelot, A. Tamke, T. Dang, and G. Breuel, "Handling uncertainties in criticality assessment," in *2011 IEEE Intelligent Vehicles Symposium (IV)*, June 2011, pp. 571–576.

[8] A. Philipp and D. Goehring, "Analytic collision risk calculation for autonomous vehicle navigation," in *2019 International Conference on Robotics and Automation (ICRA)*, May 2019, pp. 1744–1750.

[9] A. Pierson, W. Schwarting, S. Karaman, and D. Rus, "Navigating congested environments with risk level sets," in *2018 IEEE International Conference on Robotics and Automation (ICRA)*, May 2018, pp. 5712–5719.

[10] ——, "Learning risk level set parameters from data sets for safer driving," in *2019 IEEE Intelligent Vehicles Symposium (IV)*, June 2019, pp. 273–280.

[11] R. Altendorfer and C. Wilkmann, "What is the collision probability and how to compute it," *CoRR*, vol. abs/1711.07060, 2017. [Online]. Available: http://arxiv.org/abs/1711.07060

[12] M. Althoff and S. Magdici, "Set-based prediction of traffic participants on arbitrary road networks," *IEEE Transactions on Intelligent Vehicles*, vol. 1, no. 2, pp. 187–202, June 2016.

[13] J. Kim and D. Kum, "Collision risk assessment algorithm via lane-based probabilistic motion prediction of surrounding vehicles," *IEEE Transactions on Intelligent Transportation Systems*, vol. 19, no. 9, pp. 2965–2976, Sep. 2018.

[14] R. Krajewski, J. Bock, L. Kloeker, and L. Eckstein, "The highd dataset: A drone dataset of naturalistic vehicle trajectories on german highways for validation of highly automated driving systems," *CoRR*, vol. abs/1810.05642, 2018. [Online]. Available: http://arxiv.org/abs/1810.05642

[15] F. Poggenhans, J. Pauls, J. Janosovits, S. Orf, M. Naumann, F. Kuhnt, and M. Mayr, "Lanelet2: A high-definition map framework for the future of automated driving," in *2018 21st International Conference on Intelligent Transportation Systems (ITSC)*, 2018, pp. 1672–1679.

[16] R. S. Sutton and A. G. Barto, *Reinforcement learning: An introduction*. MIT press, 2018.

[17] V. Dixit, S. Chand, and D. Nair, "Autonomous vehicles: Disengagements, accidents and reaction times," *PLOS ONE*, vol. 11, p. e0168054, 12 2016.

[18] M. Abadi, A. Agarwal, P. Barham, E. Brevdo, Z. Chen, C. Citro, G. S. Corrado, A. Davis, J. Dean, M. Devin, S. Ghemawat, I. Goodfellow, A. Harp, G. Irving, M. Isard, Y. Jia, R. Jozefowicz, L. Kaiser, M. Kudlur, J. Levenberg, D. Mané, R. Monga, S. Moore, D. Murray, C. Olah, M. Schuster, J. Shlens, B. Steiner, I. Sutskever, K. Talwar, P. Tucker, V. Vanhoucke, V. Vasudevan, F. Viégas, O. Vinyals, P. Warden, M. Wattenberg, M. Wicke, Y. Yu, and X. Zheng, "TensorFlow: Large-scale machine learning on heterogeneous systems," 2015, software available from tensorflow.org. [Online]. Available: http://tensorflow.org/

[19] S. Shalev-Shwartz, S. Shammah, and A. Shashua, "On a formal model of safe and scalable self-driving cars," *CoRR*, vol. abs/1708.06374, 2017. [Online]. Available: http://arxiv.org/abs/1708.06374

[20] M. Werling, J. Ziegler, S. Kammel, and S. Thrun, "Optimal trajectory generation for dynamic street scenarios in a frent frame," in *2010 IEEE International Conference on Robotics and Automation*, May 2010, pp. 987–993.